A Computational Methodology for Estimating the Detected Energy Spectra of the Gamma-Ray Flux From Irradiated Nuclear Fuel

L. Senis, Z. Elter, V. Rathore, E. Andersson Sundén, P. Jansson, S. Holcombe, M. Åberg Lindell, A. Håkansson, and P. Andersson

***Abstract*— Gamma-ray spectrometry using collimated detectors is a well-established examination method for irradiated nuclear fuel. However, the feasibility of examining a particular nuclide of interest is subject to constraints; the peak must be statistically determinable with the desired precision, and the total spectrum count rate in the detector should not cause throughput issues. Methods were assembled for gamma spectrum prediction to optimize instruments for gamma emission tomography and to enable *a priori* feasibility evaluation of determination of single peaks of irradiated nuclear fuel. The aim was to find reliable results (∼10% accuracy) regarding total spectrum and peak count rates with faster computation time than a full-Monte Carlo approach. For this purpose, the method is based on depletion calculations with SERPENT2, a point-source kernel method for the collimator response, and a rig response matrix and a detector response matrix, both computed with MCNP6. The computational methodology uses the fuel properties (dimensions, materials, power history, and cooling time) and the instrumental setup (collimator and detector dimensions and materials) as an input. The prediction method was validated using the measured data from a high-burnup, short-cooled test fuel rodlet from the Halden reactor. Absolute count rates and ratios of characteristic peaks were compared between predicted and measured spectra, showing a total count rate overestimation of 7% and discrepancies between 2% and 20% for the single peaks (the same order of magnitude of the uncertainty). This level of agreement is deemed sufficient for measurement campaigns planning and the optimization of spectroscopic instruments for use in gamma scanning and tomography of nuclear fuel.**

***Index Terms*— Gamma emission tomography (GET), gamma spectroscopy, nuclear fuel inspection, post irradiation examination (PIE).**

I. Introduction

GAMMA scanning and gamma emission tomography (GET) are techniques for nondestructive assay of irradiated nuclear fuel [1]–[3]. These techniques present the valuable possibility to noninvasively obtain data regarding the fuel state and its nuclide composition [4], [5] but also for the validation of the burnup and power distribution [6], [7]. Other uses are the determination of fission gas release fraction [8] or the extent of fragmentation and relocation of nuclear fuel caused by in-pile transients [9].

Due to the high activity of irradiated nuclear fuel (in the order of 100 TBq/kg [10]), gamma scanning setups, as well as GET detector setups, include long collimators [2] to be selectively sensitive to a small part of the fuel, while benefiting from thick radiation shielding of the unwanted radiation from other parts of the fuel.

For *a priori* evaluation of the feasibility detection (or quantitative determination) of a particular radionuclide, either with gamma scanning or GET, some challenges present themselves. First, the gamma-ray intensity of the particular nuclide needs to be strong enough to provide a statistically relevant signal in the presence of background. In a single measurement, this can be determined, e.g., by Currie's [11] decision limits. However, this is further complicated in the case of nuclear fuel, where the background may largely come from other nuclides that are present in the same fuel sample. The gamma-ray background can thus not be characterized only using a background spectrum recorded in the lab, but one must also consider the multitude of gamma-ray emitters that are produced in the nuclear fuel itself. This is in turn dependent on the power history and the cooling time, which is specific for each fuel sample.

The detectability of specific nuclides may be difficult to judge in case of several circumstances, if:

1) The nuclear fuel is short-cooled, and many radioactive species are still present.
2) It has a peculiar irradiation history.
3) The nuclide of interest is not one of the dominating peaks in the spectrum.
4) The gamma-ray energy of the nuclide is in a region with a nonnegligible continuum or peak background from other nuclides.

Furthermore, reference fuel spectra of relevance may not be available when designing new instruments or they do not allow to assert the sensitivity performance in case of relevant variations in setup parameters.

Manuscript received October 5, 2021; revised January 27, 2022; accepted February 11, 2022. Date of publication February 16, 2022; date of current version April 19, 2022. This work was supported by the Swedish Foundation for Strategic Research under Grant EM-16-0031.

L. Senis, Z. Elter, V. Rathore, E. Andersson Sundén, P. Jansson, A. Håkansson, and P. Andersson are with the Division of Applied Nuclear Physics, Department of Physics and Astronomy, Uppsala University, 75236 Uppsala, Sweden (e-mail: lorenzo.senis@physics.uu.se).

S. Holcombe and M. Åberg Lindell are with the Institute for Energy Technology, 1777 Halden, Norway.

Color versions of one or more figures in this article are available at https://doi.org/10.1109/TNS.2022.3152264.

Digital Object Identifier 10.1109/TNS.2022.3152264

Generally, judging the feasibility of peak interrogation in such cases requires the prediction of three count rates: the signal count rate of the peak itself, the background count rate in the peak region, and also the total count rate. The two former are needed to ensure that the peak is statistically significant, while the latter is needed to ensure that count-rate limitations of the detector system are not exceeded. The method presented in this work aims to predict gamma-ray spectrum in a collimated detector system, based on the input of the fuel dimensions and material, power history, collimator dimensions, and detector type and geometry.

While it is also possible to predict detector spectrum and count rates using standard Monte Carlo (MC) tools, the transport of photons through long and thin collimators can make the MC method prohibitively time-consuming, due to the low probability of the gamma ray reaching the detector.

This work aims to overcome this issue by presenting a hybrid method, which combines MC-based methods using SERPENT2 [12] and MCNP6 [13], here used for calculating the depletion/activation of the fuel, the intrinsic detector response, and the rig response (which includes the self-attenuation and buildup of scattered photons). However, the standard MC methods are replaced with a recently developed point-source kernel method [14], using analytical expressions for the collimator response, assuming the optical field of view, and neglecting the transmission through the collimator bulk material (systematic effects in the results due to this assumption will be discussed in Section III-D). Thereby, relatively fast execution of the spectrum prediction is allowed (as shown in [14]), which is useful when exploring a broad range of experimental configurations, e.g., for the optimization of a setup.

This article presents the methods for predicting the gamma-ray spectrum, and the predictions are benchmarked using a spectrum obtained in Halden from fuel that is representative of the planned use, a high-burnup, short-cooling time transient test rod. The proposed method will be used in particular for the optimization of a planned tomography system for high-spatial-resolution GET [15], [16]. However, the methods for spectrum prediction may be also useful, in general, in the planning of gamma scanning and GET campaigns at research reactors, commercial reactors, or hot cell facilities.

II. Outline of the Method

To predict the detector spectrum, several computational steps need to be taken.

1) *Depletion:* Due to the irradiation of the fuel during the in-reactor operation, the nuclear fuel is depleted, and several gamma-emitting radionuclides are created due to various transmutation reactions, in particular fission. The transmutation continues due to radioactive decay after the irradiation has ended. At the time of inspection, the properties of interest are given by the nuclide vector and corresponding nuclide activities. The gamma lines (energies and intensities) constitute the gamma emission spectrum. In this work, the SERPENT2 [12] code has been used to perform the depletion calculation and to calculate the gamma emission spectrum.
2) *Self-Attenuation and Buildup:* Due to the high density of the fuel itself, in combination with the use of surrounding structures, such as cladding and fuel-rig features, such as a shroud, the emitted spectrum is highly modified by attenuation. This attenuation has the consequence that the line intensities decrease, but also causes a continuum background, due to the emergence of a scattered gamma-ray flux. In this work, a rig response was calculated using MCNP6 [13]. The energy distribution of escaping photons from the fuel-containing test rig was obtained for varied source gamma-ray energy and varied scattered gamma-ray energy, resulting in a rig response matrix.
3) *Collimator Response:* The collimator response is typically a relevant factor in gamma-ray transport problems, reducing throughput flux in the detector by several orders of magnitude by shielding radiation from unwanted origin or in an unwanted direction. Because of the low probability per starting photon to be transmitted through the collimator, the MC method tends to be inefficient at calculating this effect. For fast computation, the optical contribution model of [14] was applied. This model assumes an ideal absorbing collimator bulk, with a rectangular cross-sectional slit. It should be noted that this idealization neglects the transmission through collimator material and effects of scattering therein.
4) *Detector Response:* Finally, the detector response to the incoming photons needs to be considered. The response was modeled for photons of varied energy with MCNP6, using a monodirectional point source to mimic the collimated beam hitting the detector, resulting in a detector response matrix.

Further details of computation steps I–IV are described in Sections III-A–III-D. It can be noted that the conceptual division of the calculation is providing some modularity. Often, a small number of fuel test rigs are exploited in, e.g., a material test reactor, and similarly, a small number of detectors are available. Therefore, the calculations for steps II and IV, while requiring some effort and time, can be reutilized in future evaluations for other fuel specimens.

A. Depletion Calculation and Gamma Emission Spectrum

After the irradiation, the fuel includes several gamma-emitting radionuclides. The activity of each nuclide is organized in a multielement vector A defined as

$$A_{i=1:N} = [A_1, A_2, \ldots, A_N] \tag{1}$$

where A_i is the activity per nuclide i and N is the total number of radioactive nuclide species contained in the irradiated fuel. Each radionuclide may in principle present multiple emission lines, each with a specific emission probability I_γ. The emission lines can be indexed by $j = 1{:}J$, where J is the number of gamma lines for the specific ith radionuclide. The emission

intensity per line, H_j, can be expressed as

$$H_j = \sum_{i=1}^{N} \left(DA_i * I_{\gamma i,j} \right) \tag{2}$$

where D is the correction factor, expressed in (3), needed for the conversion of the activity per unit length [Bq/cm] obtained by SERPENT2, to a planar activity concentration [Bq/cm^2] in field of view of the collimator slit (which is the required input of the optical contribution model). The approximation of the rod as a planar source as in [14] has been considered valid due to the collimator dimensions. The slit is much longer in comparison to its height and its width (as shown in Table I) and projects a field of view with a small divergence, smaller than the diameter of the rod. Thereby, from the detector point of view, the rod would appear in good approximation as a plane with isotropic emission. For a small collimator viewing the center of a fuel rod, the value of D can be estimated by (see derivation in Appendix A)

$$D = \frac{2}{\pi R_{\text{pellet}}}. \tag{3}$$

The nuclide inventory may present thousands of gamma-line emissions with a wide range of emission rates. However, many of these are of low energy or intensity and are unlikely to escape the sample and reach the detector.

B. Rig Response

The gamma rays generated in the fuel have a certain probability to scatter or being absorbed while traveling through the fuel sample and the surrounding structures. The magnitude of these effects depends on gamma energy and the materials and dimensions of the fuel sample and rig. The scattered gammas can still be detected and contribute to the spectrum continuum, potentially hiding peaks of interest and increasing the total spectrum count rate, which may affect the throughput. Therefore, it is desired to include this component in the spectrum prediction.

To calculate these contributions, a matrix, S, is created where the elements $s_{g,j}$ represent the probability per starting gamma ray from the fuel of gamma line j, exiting the rig at the energy interval g is reported, where $g = 1{:}G$ is the index on the energy discretization applied in the simulation output

$$S = \begin{bmatrix} s_{11} & s_{12} & s_{13} & \cdots & s_{1J} \\ s_{21} & s_{22} & s_{23} & \cdots & s_{2J} \\ s_{31} & s_{32} & s_{33} & \cdots & s_{3J} \\ \vdots & \vdots & \vdots & \vdots & \vdots \\ s_{G1} & s_{G2} & s_{G3} & \cdots & s_{GJ} \end{bmatrix}. \tag{4}$$

Each element of $s_{g,j}$ represents the rig response to a particular gamma source-line energy. For elements $s_{g,j}$ for which the line energy j is within the exit energy bin g, such that $E_{g-1} < E_j \leq E_g$, the rig response is simply understood as the attenuation, α_j, of the gamma line in the fuel object (although some amount of small-angle scattered photons may also be added in this bin). For cases where $E_j < E_{g-1}$, the elements $s_{g,j}$ represent buildup, $\beta_{g,j}$, caused by scattering (including other interactions) in the fuel rig and exiting at the particular energy interval g. Finally, for $s_{g,j}$, such that $E_g > E_j$, the elements are zero, since interactions of the gamma in the fuel cannot increase the gamma-ray energy (however, with the possible exception for photonuclear reactions that may become relevant for high-energy gamma rays).

TABLE I

TABLE SUMMARIZES THE DIMENSIONAL PARAMETERS OF THE INSTRUMENTAL SETUP (SAMPLE, COLLIMATOR, AND DETECTOR) USED AS A VALIDATION TEST

Parameter	Value [mm]
Fuel radius	4.1
Fuel-cladding gap	0.03
Cladding thickness	0.5
Heat cylinder inner radius	10
Heat cylinder thickness	3.1
Pressure cylinder inner radius	17
Pressure cylinder thickness	3
Collimator mean length	705
Slit width	1
Slit height	2
Detector radius	25
Detector height	50
Dead layer thickness	0.7
Cold finger radius	4
Cold finger height	30

It can be noted that if the same energy bins would be used for the source energy and the exiting gamma energy, the matrix S would be upper triangular. However, this is not necessarily the case, and in this work, we used the SERPENT2 output's gamma lines for E_j, which is in turn based on the JEFF-3.3 library. In contrast, we have used the energy binning g based on a constant interval.

For each gamma line j, the attenuation and buildup coefficients, α_j and $\beta_{g,j}$, were calculated using two different MCNP simulations, using the photon current tally F1 [13]. The attenuation elements, α, were calculated by setting a monodirectional and monoenergetic-biased source, limited for the fuel inside the field of view of the slit. This source representation has been considered appropriate due to the long distance between the fuel and the detector, which is much bigger than the detector dimensions (see Table I). The measurement is, therefore, a far-field measurement where it is possible to assume that all emitted gamma rays hit the detector surface perpendicularly. The result represents the probability per full-energy gamma ray, that is emitted in the favorable direction of the slit, to exit the fuel object. This approach gives a precise prediction for the full-energy peak intensities (as shown in [14, Sec. 5]). It is also a rapid calculation performed by the MC technique, since the probability of successfully exiting the fuel rig is several tens of percent for relevant gamma-ray energies.

However, as noted above, the buildup caused by gamma rays scattered in the object cannot be evaluated with this simulation, due to the buildup potentially originating far away from the collimator opening and with arbitrary starting direction, and this is not modeled in the simulation. Therefore, a second simulation with MCNP was used, with an isotropic, large-volume source correspondent to the axially extended fueled region of the sample. Exploiting the symmetries of the fuel

object to speed up the MC calculation, the exiting photons were tallied when exiting the fuel object along its entire height. This greatly speeds up the convergence of the simulation, as compared with having the tally made only in a limited collimator slit opening. The photons able to escape from the bulk material were tallied with energy and directional binning, where the directional binning was used to select photons only within a limited acceptance angle, intended to mimic the cone view of the narrow collimator. The exit probability per starting photon was recorded per starting energy and per exiting energy, inside the acceptance angle. The output of the buildup simulation is the probability per starting photon to exit the fuel rig in the perpendicular direction, per starting photon, and per exit energy bin g, for the entire height of the fuel rig, $\gamma_{g,j}$. It can be noted that for the evaluation of the property of interest, $\beta_{j,g}$, a renormalization is needed, considering that the rig response needs to be normalized per gamma ray transmitted in a favorable direction toward the collimated detector. For this purpose, a scaling factor is evaluated using the full-energy bin of the buildup simulation and the priorly calculated attenuation of the directly transmitted intensity, α_j. This results in a scaling factor Y for each line energy j, such that

$$Y_j = \frac{\alpha_j}{\gamma_{\acute{g},j}} \tag{5}$$

where $\acute{g}$ is the energy bin corresponding to the full-energy peak. Finally, the scattering elements, $s_{g,j}$, of the matrix S can finally be calculated as

$$s_{gj} = Y_j \gamma_{g,j}. \tag{6}$$

It can be noted that the chosen energy discretization has effects on the statistics of each bin, with a higher uncertainty for a smaller bin size, requiring compensation by a larger number of particles generated in the MC transport simulation. A possible energy discretization strategy uses the multichannel analyzer (MCA) of the detector setup. Any finer energy information is redundant, since it would be lost during the data acquisition in an experiment.

C. Collimator Efficiency

The gamma rays exiting the object need to pass through the collimator, which further reduces the intensity reaching the detector. In this process, the magnitude of the transmitted intensity is highly dependent on the slit dimensions. The emission intensities were multiplied by the geometric efficiency of the collimator, ε_{col}, calculated using the optical contribution model presented in [14]

$$\varepsilon_{\text{col}} = \frac{w^2 h^2}{4\pi L^2} \tag{7}$$

where w is the width of the slit, h is the height, and L is its length. As anticipated in Section II, the model calculates the collimator response assuming the source as an isotropic plane with certain surface activity.

In this work, the collimator response is thus treated as a simple scaling factor reducing the intensity of the entering gamma-ray spectrum. No additional buildup from the collimator itself, or transmission through the bulk material, is considered. While this is a simplification, it was shown in [14] that this is a good approximation for long collimator slits, such as often used in scans of nuclear fuel. This has also been confirmed that calculating the magnitude of buildup from a collimator with the same dimension is presented as the benchmark case (Table I in Section III). In simulations of gamma rays from hundreds to thousands of kiloelectronvolt passing a tungsten collimator, the contribution of gamma rays scattered in the collimator bulk was consistently below 3% of the events present in the full-energy peak intensity, and this was deemed negligible.

D. Detector Response

Finally, the detector response needs to be accounted for, which was done by applying a response matrix, Q_{kg}. Modeling a realistic detector geometry in MCNP, simulations were performed to obtain the energy deposition spectrum, to varied incident energy. Accounting in a simplified manner for the collimator, the source is modeled as a monoenergetic monodirectional gamma ray hitting the detector centrally and perpendicularly to the detector wall, which mimics a small-width collimated beam pointed straight toward the detector. The simulation was repeated with varied source energy to obtain the energy-dependent response, and the pulse-height distribution (i.e., using the tally eight feature of MCNP [17]) in the detector crystal is obtained. The results do not include the simulation of the detector charge collection process and the possible readout effects, other than an energy-dependent broadening, as described in Section II-E. The discretization used for the output can (again) be defined accordingly to the binning inherent in the MCA, using the index k for this discretization, in addition to the incident gamma-ray energy discretization indexed by g, being the same index as previously used for the gamma-ray energy spectrum exiting the fuel rig.

It can be noted that while a large number of MC transport simulations are needed to obtain the detector response matrix according to the description above, this can be performed very rapidly if using an automated script, since the individual simulation runs fast, owing to the high efficiency of a detector to a collimated beam, i.e., in particular, the low-efficiency process of the collimation was excluded from the MC model to save computation time, since every modeled gamma ray will hit the detector at the very least its casing. In addition, it can be noted that this use of a detector response provides some modularity, since the detector may often be reused, for new fuel samples and new collimators.

E. Full Pulse-Height Spectrum Formulation

The different phenomena described in detail in the previous sections can be expressed mathematically in a condensed formula. Using already defined terminology, the count rate, P_k, of MCA of bin k can be expressed as

$$P_k = \sum_{g=1}^{G} \left(Q_{k,g} * \varepsilon_{\text{col}} \sum_{j=1}^{M} \left(H_j * s_{gj} \right) \right) \tag{8}$$

with a linear combination of the gamma emission intensities H_j, the collimator efficiency ε_{col}, absorption and scattering

response matrix, S_{gj}, and detector response matrix, Q_{kg}. It can be noted that the $\sum_{j=1}^{M}(H_j * s_{gj})$ term gives a vector as a result, which can be interpreted as the distribution of the scattered gamma rays from the fuel object. Applying the collimator efficiency factor, ε_{col}, the intensities are scaled considering the collimator effect in reducing the incoming gamma flux (however, neglecting buildup from the collimator itself). Because the response of the detector depends on its characteristics and the incident gamma energies, this is convoluted with the detector response matrix, Q_{kg}, to get a realistic prediction of a pulse height spectrum.

The terms of (8) are described in detail in (2), (6), and (7), showing their dependence on, e.g., the collimator slit and sample rod dimensions or the nuclide activities. Substituting into (8) the previous expressions and accounting for also the time of the interrogation, t, the counts collected per channel can be predicted according to the comprehensive expression in the following equation:

$$P_k t = \frac{w^2 h^2}{4\pi L^2} \frac{2t}{\pi R_{\text{pellet}}} \sum_{g=1}^{G} \left(Q_{k,g} \sum_{j=1}^{M} \left(\sum_{i=1}^{N} \left(A_i * I_{\gamma i,j} \right) * Y_j c_{gj} \right) \right) \tag{9}$$

showing explicitly the expected number of events in each energy interval of the detected spectrum. For the calculation of the entire pulse height spectrum, the calculation is repeated for $k = 1{:}K$.

Finally, the variabilities of charge-carrier production and collection in the detector may be considered, resulting in the broadening of the peaks. A Gaussian broadening was convoluted with the full spectrum calculated according to (9), where the full-width at half-maximum (FWHM) was modeled with a linear dependency on the energy, following the suggested fit in [18, Table 6.4].

III. Validation Test Parameters

A. Instrumental Setup

The model proposed in Section II has been validated using a spectrum acquired during a measurement campaign performed with the GET setup present at the Halden boiling water reactor (HBWR). In particular, this campaign was performed on a high-burnup fuel rodlet subjected to an in-pile loss of coolant accident (LOCA) transient test.

This type of test object represents a couple of challenges when planning the interrogation, and a long and thin custom-made collimator was used, with correspondingly a low efficiency, prohibiting fast evaluation of gamma-ray intensity using MC methods.

In addition, the spectrum is complex, with a mixture of gamma rays of short-lived and long-lived radionuclides owing to a highly unique burnup history with long interruptions in the power history and short cooling time since the end of irradiation. Because of this, *a priori* anticipation of the spectrum and count rate is challenging, unless with methods such as described in this work.

The test rodlet used an axial section of a pressurized water reactor (PWR) pin as a sample (fuel radius of 4.1 mm with a cladding thickness of 0.500 mm). The pin section was inserted in a test rig having two concentric cylinders, a heater cylinder made in Zircaloy[1] (Zirc-2 [19]), and a pressure cylinder made of stainless steel, both of them with a thickness of about 3 mm. A third cylinder was also present during the irradiation test but removed in the measurement phase. The collimator used was made in DENSIMET[1] (tungsten alloy with percentage fractions of nickel and iron) and presented a rectangular slit with 1 mm of width and 2 mm of height. It can be noted that the rectangular collimator had a slight difference in the length between the vertical and horizontal constraints, which were 655 and 755 mm apart,, respectively. However, the optical model of [14] is expressed for an identical length between these constraints, which therefore was obtained by using the average, 705 mm. The high purity germanium (HPGe) detector used a Canberra model GC2018, coaxial, p-type [2] (crystal radius and height are, respectively, 25 and 50 mm) cooled with liquid nitrogen and coupled with an Ortec D-Spec-50 MCA. The MCNP model of the detector is presented in Fig. 1. The spectrum was acquired with the slit laterally positioned centrally to the rodlet sample.

A schematic representation of the instrumental setup is reported in Fig. 3, while the dimensions used are summarized in Table I.

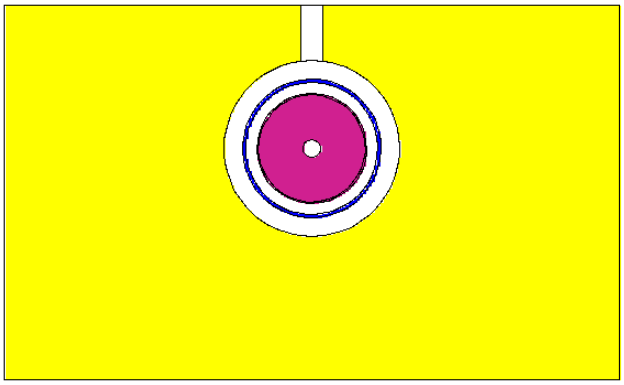

Fig. 1. MCNP representation of HPGe model used showing germanium crystal (purple), an aluminum cap (blue), and the surrounding shielding of steel (yellow).

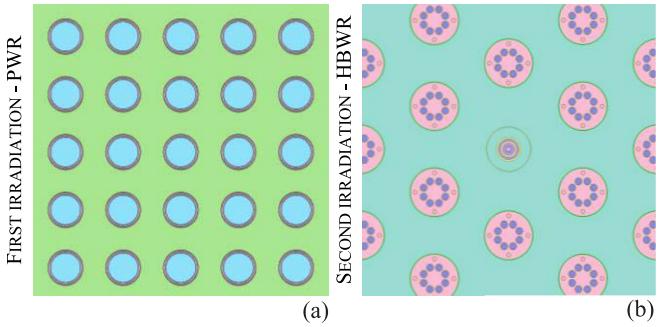

Fig. 2. Simplified SERPENT2 reactor models of the (a) first and (b) second irradiation periods. For the first irradiation, the rod is inserted in an infinite PWR 2-D fuel pin lattice and the burnup is simulated according to the LHGR distribution shown in Table II. The composition of the fuel after the first irradiation, including decay time, was used for the second irradiation model shown on the right, which simulates the rodlet and surrounding rig in the center of a boiling heavy-water reactor core configuration.

[1]Register Trademark.

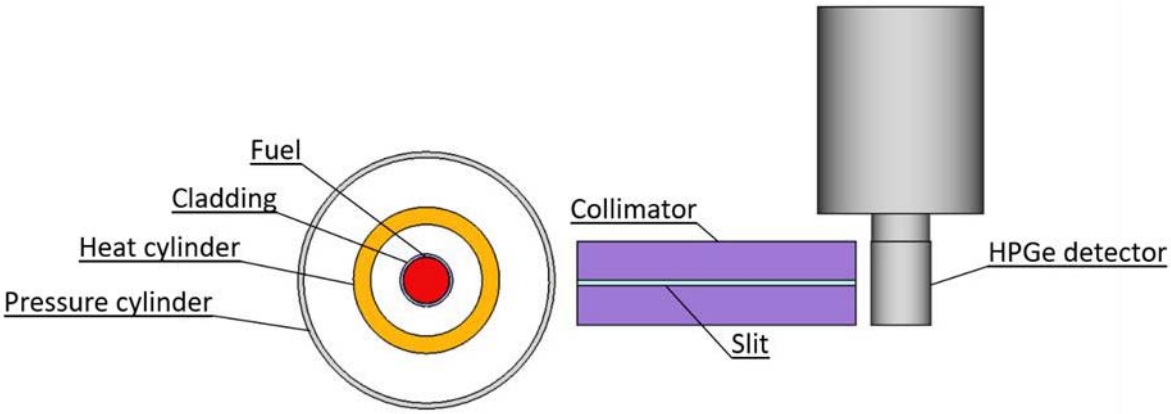

Fig. 3. Representation of Halden GET measurement setup (not-to-scale). The irradiated sample consists of a rodlet of a PWR fuel pin (in red), incapsulated into two cylinders (yellow and light gray) serving as heater and pressure pipe. The collimator presents a rectangular slit constrained by DENSIMET blocks (in light blue). At the end of the slit, an HPGe detector is present.

B. Simulation Parameters

The power history and the cooling periods for the fuel were available and used in the calculation, according to Section II-A. Starting with an initial enrichment of 3.8%, the first irradiation period covers five reactor cycles in a PWR reactor. The detailed power distribution was simplified to constant power cycles using the average linear heat generation rate (LHGR) for these five cycles, with a total exposure achieved of 60 GWd/tU. After the first irradiation, the rod was stored for 12 years and then cut to obtain the smaller rodlet. The rodlet was subjected to a second irradiation of three days in the Halden Boiling Water research reactor (25 MW_{th}) for a LOCA transient test. Finally, after 14 days of cooling, the sample was measured. The depletion models were realized in SERPENT using an infinite 2-D lattice, one for each reactor type, as shown in Fig. 2, while the simulated burnup history is summarized in Table II.

The burnup simulations in SERPENT2 were made with 10 000 neutrons per generation, with 20 inactive cycles and 500 active cycles, using the cross-sectional library JEFF-3.3. To estimate the uncertainty of the simulations, 100 repeated simulations were performed. The mean values of the activities were used for estimation and their standard deviation as an uncertainty estimate for the precision type errors induced by the MC random sampling.

From the gamma-line catalog obtained in the SERPENT output, the 2000 strongest intensity gamma lines above 50 keV were selected, which corresponded to the 61 highest intensity nuclides. The remaining gamma-ray lines of lower intensity were neglected.

In the rig response evaluation according to Section II-B, the buildup was modeled in MCNP6.2 with an acceptance angle of 7.5° off the normal to the collimator front surface. This was sufficient to fully cover the collimator slit's entrance with some margin.

C. Analysis of Measured Spectrum

The measured spectrum from a 30-s interrogation was analyzed, and for each peak observed, its number of counts was calculated. This was obtained by summing the counts for each of the channels in a window corresponding to 2∗FWHM of the peak (which includes more than 98% of a Gaussian distribution). Continuum background was subtracted based on symmetric regions of interest on each side of the peak centroid, where an equal number of channels were used for background and peak centroid. The net peak area, N [counts], was calculated according to $N = P - B - (P_{\mathrm{BG}} - B_{\mathrm{BG}})$, where P is the area of the peak centroid and B is the total number of counts in the background windows. In addition, the net counts were corrected for peak background based on a background spectrum measured with the collimator outside of the fueled region for the same duration. The terms P_{BG} and B_{BG} refer to the peak centroid and background counts in this unfueled background spectrum. It can be noted that the peak background was evident in particular in the ^{137}Cs peak, but the procedure was performed for all peaks. The uncertainty of the measured peaks was estimated as

$$\sigma_N = \sqrt{P + B + P_{\mathrm{BG}} + B_{\mathrm{BG}}}. \tag{10}$$

For the predicted spectrum, the peak and background counts were estimated using the same channel window locations as used in the measured spectrum.

D. Notes on Simplifications and Sources of Error

In applying the method, some assumptions have been made.

1) Effects of fuel relocation. It should be noted that transient test rods are typically exposed to cladding ballooning, which in turn allows for relocation of some fuel and accumulation of activity in parts of the axial height of the rodlet. Correspondingly, other locations may be evacuated by the fuel. While this may be important to plan for in a gamma scanning or tomography campaign, we have not aimed to include relocation models in the spectrum prediction. Therefore, as described above, we selected to extract a validation spectrum from a collimator position with the top pellet in view. At the top of the fuel rodlet, due to the smaller heat load in the transient, no important impact on the validation data is expected due to fuel relocation in this fuel sample [20]. Self-attenuation and the buildup were

TABLE II
SIMPLIFIED CYCLE AVERAGED POWER HISTORY USED IN THE DEPLETION CALCULATION

	PWR						HBWR	
	First Cycle	Second Cycle	Third Cycle	Fourth Cycle	Fifth Cycle	Cooling period	LOCA test	Measure ment
Time interval (d)	365	365	365	365	365	4562	3.3	14
Power Density (W/g)	40.81	39.04	34.07	22.36	27.15	0	9.32	0

calculated assuming no deformation of the rod and no change of the fuel geometry.

2) The exact location of the collimated gamma flux in the detector crystal was not precisely known, introducing a possible source of inaccuracy in the detector response predictions. Therefore, it was assumed that the collimated photon beam incident in the center of the crystal. Varying the position in the simulation by 30 mm along the axial direction, a relative variation of 3% in the detector efficiency was observed. Similar variation was observed when varying the dimension of the beam spot from point-like up to the slit dimensions.
3) As mentioned in Sections II-3 and II-C, the full-energy contribution coming from outside the slit and penetrating the collimator bulk was not included in the model, but this component will be present in a real measurement and is energy-dependent. An evaluation of this contribution has been performed using the total contribution method presented in [14] for 662- and 1596-keV gamma rays, where the impact was +4% and +9%, respectively, for the collimator dimensions used here. It can also be noted that the vertical and horizontal constraints of the collimator slit were having different spacings in the experimental work, and therefore, the average was used.
4) It can be noted that the Bremsstrahlung contribution generated by secondary electrons was included in the rig response simulation using the thick-target bremsstrahlung approximation [17]. However, any bremsstrahlung generated by beta particles interacting in the fuel has not been included. For evaluation of its impact, the magnitude of this contribution was investigated for the four most active beta emitters in the irradiated fuel, ^{137}Cs, ^{140}La, ^{90}Y, and ^{90}Sr. The contribution of these amounted to less than 4% of the total spectrum count rate, which was deemed marginal enough for exclusion from the model.
5) It should also be noted that while the energy-line data provided by SERPENT2 output have high precision, some of this high precision is lost in the proposed method, where the response of the rig and the detector is discretized. If the resolution of peaks in close vicinity to each other is of particular interest for a planned application, one may, in principle, use smaller energy binning a selected region to facilitate this.

IV. RESULTS

A. Depletion Calculation

The depletion calculation was performed with SERPENT2 according to the burnup history reported in Section III-B, acquiring the gamma-emitters activities and their respective gamma-line energies and intensities. The emission spectrum of the fuel is reported in Fig. 4, depending on the activity of the specific radionuclide. The relative error of the depletion calculations ranges from a minimum of 0.1% to a maximum of 7.2% and accounted for the error propagation of the results. For the nuclides of interest reported in Table III, these are below 1% (e.g., ^{137}Cs 0.1% and ^{140}La 0.59%).

B. Rig Response

Self-attenuation in the sample and the associated buildup of scattered gamma rays have been calculated using MCNP6.2, as described in Section II-B, using the test rig and core geometries, as defined in Section III-A, and the rig response matrix, as shown in Fig. 5(a). For illustration purposes, a square matrix was calculated, while for the benchmark verification test, the exact value of the gamma-line energies was used for the calculations, resulting in a nonsquare matrix for the rig response.

In Fig. 5(b), the energy-attenuation curves obtained by MCNP6.2 are shown and compared to the analytical solution calculated using the Lambert–Beer attenuation law as calculated from a point in the center of the fuel pellet. From the simulations, the magnitude and energy distribution of the buildup is also obtained. It can be noted that for high-energy gammas, the number of escaping photons per starting photons can reach above 1. This can be explained considering that for high-energy photons, reactions with matter include pair production, where there is a multiplication of the photons.

C. Detector Response

The detector response matrix has been calculated using MCNP6.2, as described in Section II-D and as shown in Fig. 6(a). Because of the use of the same energy binning for the scattered gamma rays exiting the fuel rig, and for the energy deposition in the detector, the detector response matrix is a square matrix. In the matrix, it is possible to observe some structures typical of a gamma spectrum acquired by an HPGe detector, such as the full-energy peak, the Compton edge and continuum, the single and the double escape peaks, and the 511-keV annihilation peak (caused by annihilation events in, e.g., the detector casing).

The efficiency of the detector can also be obtained from the response matrix, calculated both for the full-energy peak efficiency and for the total spectrum efficiency [21] and reported in Fig. 6(b).

D. Resulting Spectrum

A predicted spectrum of 30 s was calculated using the input parameters presented in Section III [with a collimator

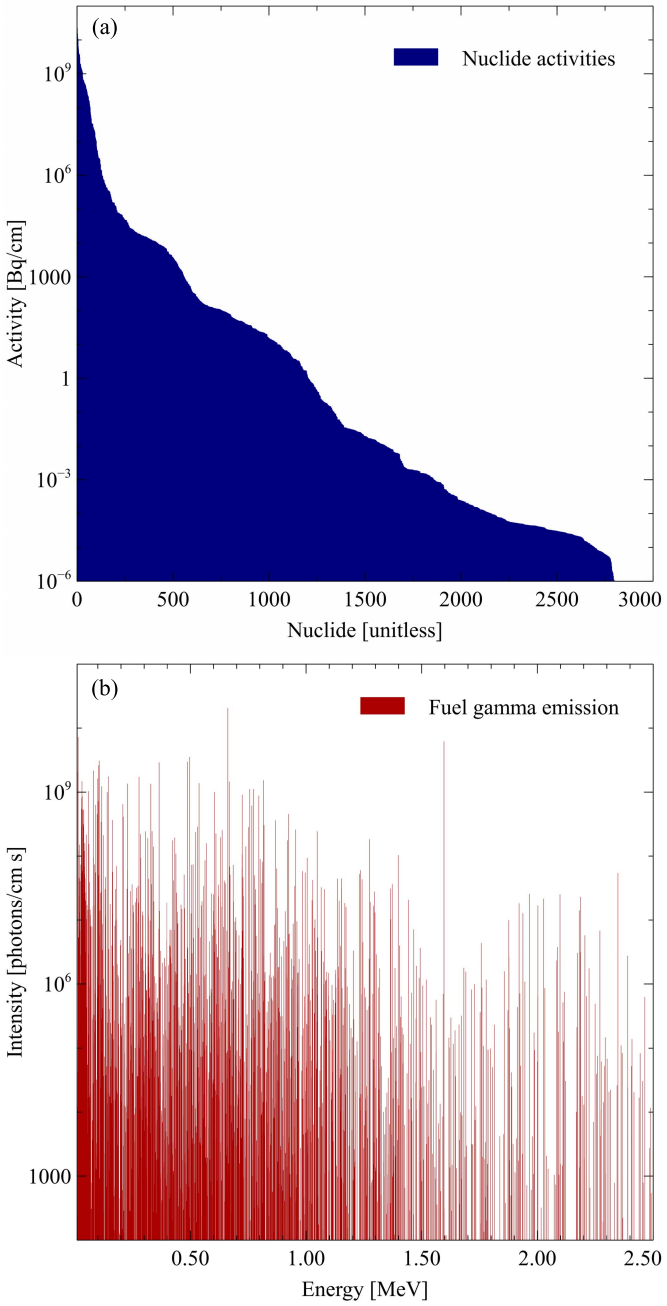

Fig. 4. (a) Activity distribution is reported for the nuclides tracked in the depletion calculation, listed from highest to lowest activity. The data are reported in decrescent order, from the most active to the less active nuclide, and it can be noted that the activities of the first 100 nuclides dominate the activity curve. (b) Gamma-line spectrum emitted from the fuel sample was calculated considering the activity of each nuclide, the number of photons emitted per decay, and the relative gamma-line emission probability per decay. The emission lines vary between almost ten orders of magnitude, where the highest is 10^{10} photons per second and cm of rod for the 662-keV gamma line of ^{137}Cs.

efficiency calculated equal to 6.36×10^{-9} using (7)] and has been compared with the measured spectrum in Fig. 7. From the results, it is possible to see that the predicted spectrum shows the typical structures of a gamma spectrum acquired with an HPGe, such as the Compton continuum, scattering events, and sharp peaks at specific energies. Correspondence between the peaks of the spectrum can also be qualitatively observed.

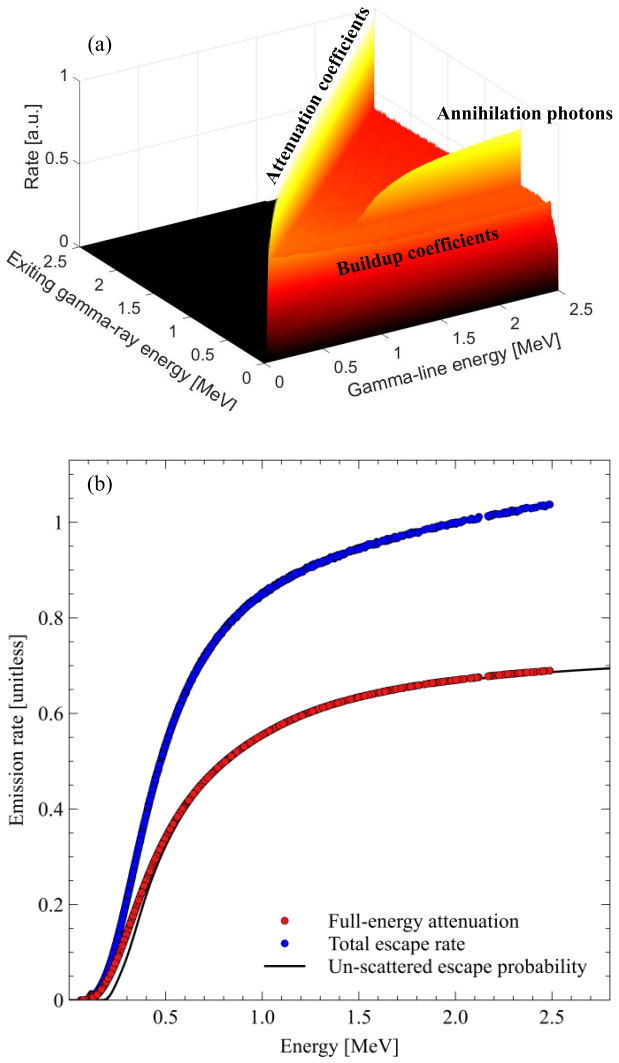

Fig. 5. (a) Rig response matrix, showing the energy distribution of the gamma rays exiting the rig as a function of source energy for illustration. It can be noted that for source energies above 1022 keV, a constant-energy feature is present at 511 keV, representing the annihilation photons escaping the rig. The color scale was selected to enhance the visibility of the full-energy transmission and the annihilation photons. (b) Escape rate per starting gamma ray is plotted: in black, for comparison, the unscattered escape probability is calculated as in [14], assuming all the activity concentrated in the center of the pellet. In red, the full-energy attenuation calculated using MCNP. In blue, the total escape rate including all energies of the escaping gamma rays.

E. Spectra Comparison

The measured spectrum was analyzed using the methodology presented in Section III-C. In general, the prediction of the gamma nuclides and the measured peak areas showed a good agreement. A similar agreement was observed in different energy ranges and for short- and long-lived nuclides. The intensities are compared in Table III with the uncertainty of 1σ obtained through applying first-order error propagation to (9), based on the uncertainties obtained in MC simulations for the calculations of the depletion (as described in Section III-B) and for the calculations of the rig and detector response. For the measured peaks, the reported uncertainty is the 1σ estimates obtained from uncertainty propagation, as presented

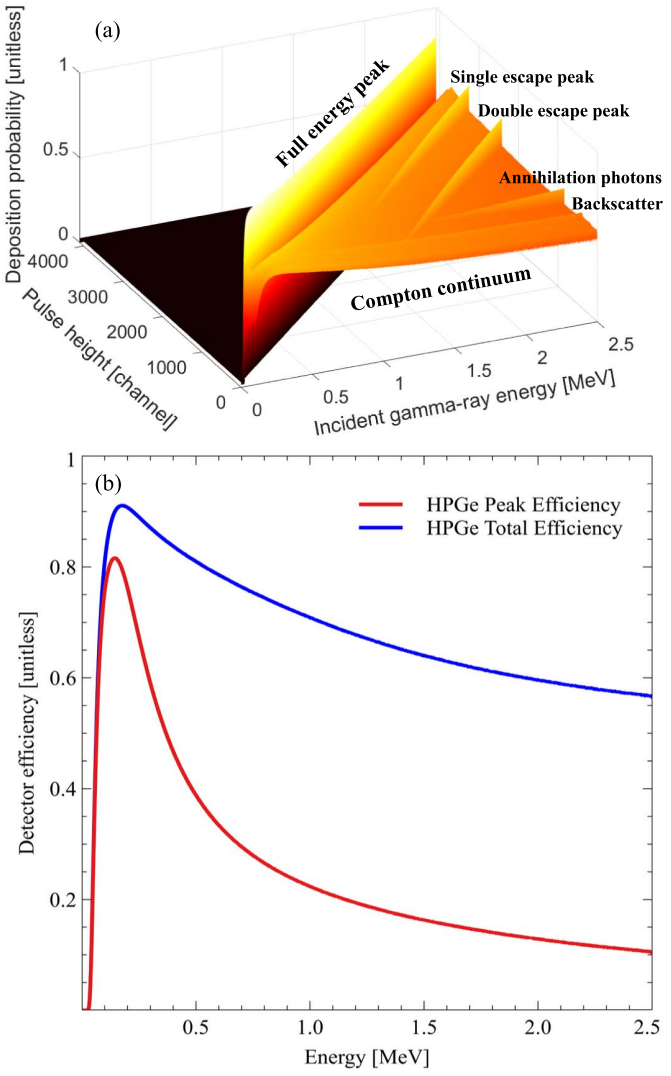

Fig. 6. (a) Detector response matrix is illustrated. Some recognizable features of HPGe detector response are evident: the diagonal features visible is the full-energy peak, while beside that, after a sharp valley, the Compton edge is noticeable. Furthermore, the double and single escape peaks are visible at constant interval from the full-energy peak. At lower energy, two more structures can be observed, represented by the annihilation peak (it can be noted it appears for gamma photons above 1 MeV), while the second smaller structure represents backscatter. (b) Detector response curves were calculated using an MCNP model the detector (Canberra GC2018). Red: full-energy peak efficiency. Blue: total spectrum efficiency.

in Section III-C. It can be noted that two peaks of ^{60}Co are visible at 1.174 and 1.332 MeV in Fig. 7. These are activation products not emitted from the fuel itself and were also present in the unfueled background spectrum. The peaks have therefore been excluded from the comparison.

A ratio was calculated between the counts of each predicted and measured peak intensity and also reported with 1σ (by the propagation of the respective uncertainties of the prediction model and the experimental results), and the ratios are provided in Fig. 8 and Table III. All the ratios have a discrepancy below 1.6σ from the ideal ratio of 1, with an average value of 1.08. It can be noticed that the method predicts a slightly higher total spectrum count (as shown in Table III).

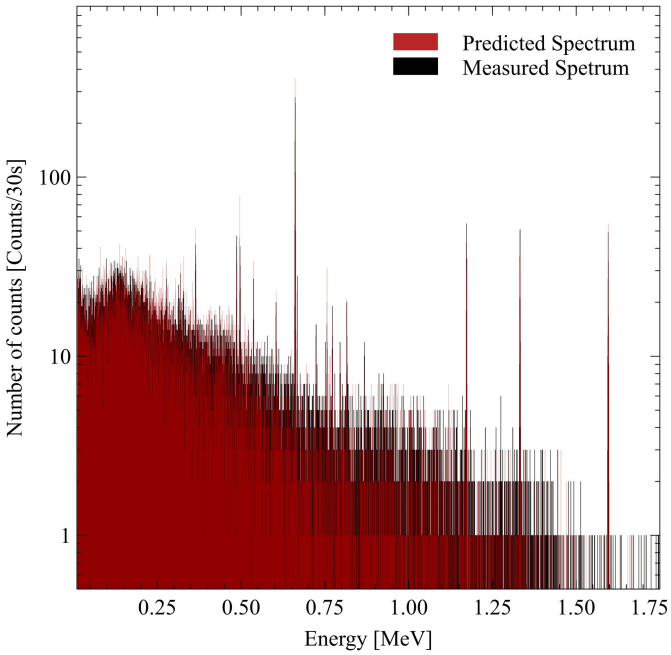

Fig. 7. Plot shows the 30-s measured gamma spectrum acquired from the GET device present in Halden and the predicted spectrum obtained from the model convoluted with a Gaussian broadening and with added Poisson noise to each bin. Note that, in addition, a spectrum collected with the fuel outside the field of view of the collimator has been added to the predicted spectrum, to include background from other sources, other than the nuclear fuel itself.

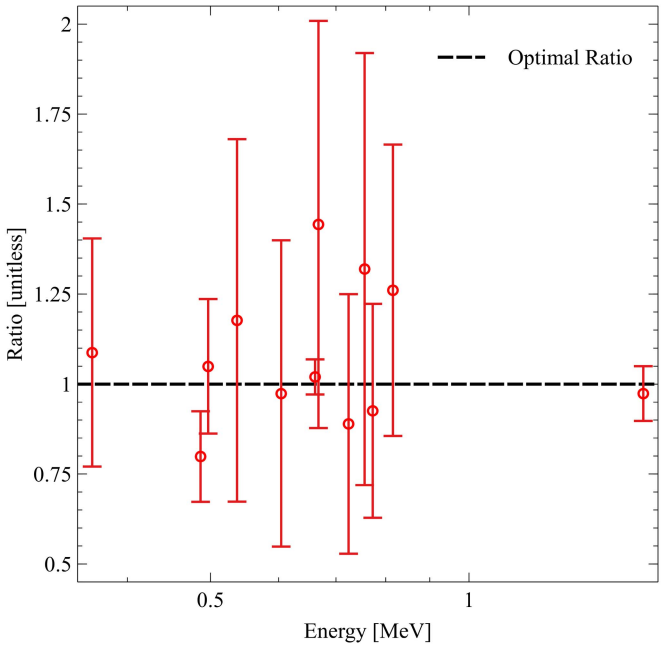

Fig. 8. Ratio values for different peak energies are plotted in logarithmic scale energy and compared to the optimal ratio value. The error bars are reported with 1σ of uncertainty and calculated through the error propagation theory of the model and measurement uncertainty. The measured values fall within 1.5σ of the prediction results.

F. Example Application in Spectrometry

The proposed method can be applied in the planning of spectroscopic measurement campaigns on nuclear fuel, predicting the detector count rate specifically in the peak of a nuclide of interest, and also enabling the estimates of

TABLE III

PEAK COUNTS COMPARISON BETWEEN THE SPECTRUM OBTAINED IN 30 S OF MEASUREMENT FOR THE PREDICTION MODEL AND FOR THE EXPERIMENTAL MEASUREMENT. THE UNCERTAINTIES ARE REPORTED WITH ONE STANDARD DEVIATION UNCERTAINTY AND FOR THE PREDICTION MODEL ARE CALCULATED THROUGH FIRST-ORDER ERROR PROPAGATION APPLIED TO (9), WHILE THE UNCERTAINTIES OF EXPERIMENTAL DATA ARE BASED ON COUNTING ERRORS IN PEAK AND BACKGROUND, AS DESCRIBED IN SECTION III. THE ENERGY OF THE GAMMAS HAS BEEN ASSIGNED TO EACH GAMMA NUCLIDE

Energy/Nuclide/Half-life	Prediction model [Counts]	Exp. Measurement [Counts]	Ratio
364 keV (^{131}I) 8 d	87.0±0.7	80±23.3	1.09±0.32
487 keV (^{140}La) 2 d	107.0±0.8	134±21.1	0.80±0.13
497 keV (^{103}Ru) 39 d	128.0±1.0	122±21.7	1.05±0.19
537 keV (^{140}Ba) 13 d	50.6±0.4	43±18.4	1.18±0.50
605 keV (^{134}Cs) 2 a	37.0±0.4	38±16.6	0.97±0.43
662 keV (^{137}Cs) 30 a	753.8±1.6	739±35.3	1.02±0.05
667 keV (^{132}I) 3 d*	53.4±0.4	37±14.5	1.44±0.57
724 keV (^{95}Zr) 64 d	32.9±0.3	37±15.0	0.89±0.36
756 keV (^{95}Zr) 64 d	40.9±0.3	31±14.1	1.32±0.60
772 keV (^{132}I) 3 d*	39.8±0.3	43±13.8	0.93±0.30
816 keV (^{140}La) 2 d	54.2±0.4	43±14.0	1.26±0.41
1596 keV (^{140}La) 2 d	159.7±1.1	164±12.8	0.97±0.08
Total spectrum counts	8948.7±3.4	8385±190.1	1.07±0.02

*(precursor ^{132}Te)

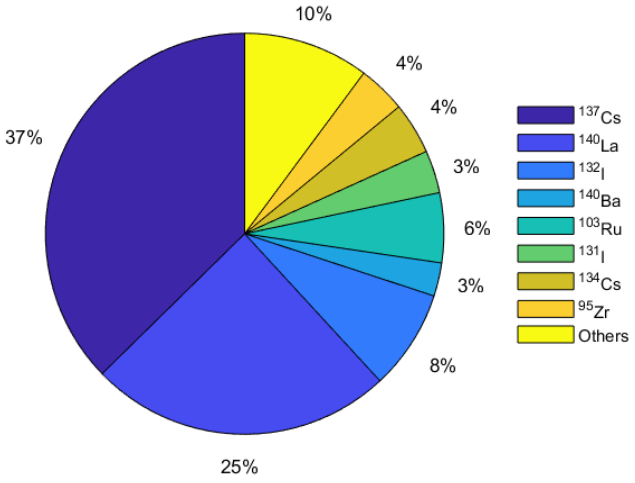

Fig. 9. Cake plot representing the contribution per nuclides to the total spectrum count rate.

TABLE IV

PREDICTED DETECTION LIMITS FOR ALL ANALYZED PEAKS, CALCULATED WITH A CONFIDENCE LEVEL OF 95%. AS CAN BE SEEN, TWO EVALUATED PEAKS DID NOT EXCEED THE DETECTION LIMIT

Peak Energy	Model Prediction	Detection Limit 95%	Detection limit passed
364 keV	87.0±0.7	63.1	Yes
487 keV	107.0±0.8	53.0	Yes
497 keV	128.0±1.0	54.0	Yes
537 keV	50.6±0.4	48.7	Yes
605 keV	37.0±0.4	45.0	No
662 keV	753.8±1.6	70.3	Yes
667 keV	53.4±0.4	37.8	Yes
724 keV	32.9±0.3	39.8	No
756 keV	40.9±0.3	34.9	Yes
772 keV	39.8±0.3	30.9	Yes
816 keV	54.2±0.4	35.1	Yes
1596 keV	159.7±1.1	7.4	Yes

continuum background in its presence and total spectrum count rate. These are the properties that affect the performance in the interrogation in terms of detectability and quantitative determinability of a peak. Since the nuclide index remaining in the comprehensive spectrum response of (9), it is possible to pinpoint and highlight the contribution of a certain nuclide. This is shown in Fig. 9, and comparing the contribution per nuclide in the spectrum is shown. The method can be applied to beforehand judge if a nuclide of interest is likely to be detected, using the so-called detection limit [18]. As reported in [18, Sec. 5.6.4] and using a $k_\alpha = k_\beta = 1.645$ (corresponding to certainty of detection of 95%), the detection limit can be calculated as $L_D = 2.71 + 4.65\sqrt{B}$, where B is the sum of the counts in the background for the expected peak region.

The demonstration of the detection limit values, as calculated using the predicted spectrum, is reported in Table IV for all peaks considered in Section IV-E. It can be noted that if compared with the predicted counts for each peak, two of the peaks were below the detection limit; thus, it could not be *a priori* ascertained with 95% confidence that these peaks would be detectable in the measured spectrum. Such *a priori* decision limits can help the spectrometry practitioner to focus limited time and resources for post irradiation examination (PIE) to feasible measurements.

V. CONCLUSION AND OUTLOOK

A hybrid model for the evaluation of gamma spectra from collimated spectrometers for nuclear fuel has been developed. Step by step, from the depletion of the nuclear fuel to calculation of gamma emission spectrum, transport through rig and collimator to the detector, and finally, the detector response is considered for *a priori* estimation of pulse height spectra. An example application was demonstrated, where a predicted spectrum was compared to an experiment.

The method utilizes fast analytical integration methods to calculate the collimator efficiency, combined with MC models for fuel activation, for gamma ray transport through fuel test rig, and detector response evaluation. The models allow the prediction of the pulse-height spectrum, and in turn, this allows

a priori evaluation of detectability and determinability of any gamma-ray peak of interest, that is generated in irradiated fuel.

The use of modular precalculated detector response, and fast analytical models for the collimator response, allows for relatively fast computations if compared to a full MC approach. The flexibility of the proposed method allows for iterative optimization procedures, e.g., the collimator selection for fuel scans, where, typically, the smaller collimator is preferred from the perspective of spatial resolution, but limits are presented by the decreasing count rate. The methods can also be used to investigate whethere a particular nuclide will be detectable and/or determinable in the complex nuclear fuel spectrum at a certain point in time or whether it will be obscured by the presence of background from other nuclides that may dominate the spectrum.

The experimental validation showed a reasonably good agreement of peak intensities, with deviations up to 20%, in the same order of magnitude as the uncertainties. The total spectrum count rate was slightly overestimated. There was a discrepancy of about 7%, which, while being a statistically significant difference, is still a small relative deviation, which is likely caused by the simplifications applied (e.g., of the margin of the angle of acceptance of the sample buildup component, and the simplified geometries used for burnup and gamma-ray transport). These factors, as well as the cycle averaging of the PWR power history, are likely contributors to the observed discrepancy between the prediction and measurement.

It is planned that the method for prediction of peak, background, and total spectrum count rates will be used in the design of new measurement setups; in particular, the study is planned for the design and optimization of a high-spatial-resolution GET system for nuclear fuel.

APPENDIX A

As described in Section II-A, a correction factor D is needed to convert the linear activity concentration of the rod, A [Bq/cm], which is the SERPENT output, to planar surface activity in front of the collimator, A_S [Bq/cm^2], as required by the optical contribution model. We obtained this conversion factor by considering the product of three factors: 1) the activity, A_d [Bq], of a disk section in the axial height range of the slit opening; 2) the fraction f of A_d that is within a rectangular prism in the view of the collimator; and 3) a normalization factor, $(1/wh)$, which is required for the cross-sectional area of the slit opening.

The fraction f can be defined as, $(2wh\,R_{\text{Pellet}}/\pi h R^2_{\text{Pellet}})$, which is the volume ratio of a rectangular prism in front of the slit opening and the volume of the whole disk of radius R_{Pellet}. The use of a rectangular prism field of view is an idealization, valid if w is small compared to the diameter of the rod, and the length of the collimator is long compared to the rod diameter. Finally

$$A_S = A_d * f * \frac{1}{wh} = hA * \frac{2w\,R_{\text{Pellet}}}{\pi R^2_{\text{Pellet}}} * \frac{1}{wh} = \frac{2A}{\pi R_{\text{Pellet}}} = DA. \tag{11}$$

Consequently, the conversion factor is $D = (2/\pi R_{\text{Pellet}})$, as presented in (3) of Section II-A.

REFERENCES

[1] P. Jansson, S. J. Svärd, A. Håkansson, and A. Bäcklin, "A device for nondestructive experimental determination of the power distribution in a nuclear fuel assembly," *Nucl. Sci. Eng.*, vol. 152, no. 1, pp. 76–86, Jan. 2006, doi: 10.13182/NSE06-A2565.

[2] S. Holcombe, S. J. Svärd, and L. Hallstadius, "A novel gamma emission tomography instrument for enhanced fuel characterization capabilities within the OECD Halden reactor project," *Ann. Nucl. Energy*, vol. 85, pp. 837–845, Nov. 2015, doi: 10.1016/j.anucene.2015.06.043.

[3] C. Willman, A. Håkansson, O. Osifo, A. Bäcklin, and S. J. Svärd, "Nondestructive assay of spent nuclear fuel with gamma-ray spectroscopy," *Ann. Nucl. Energy*, vol. 33, no. 5, pp. 427–438, Mar. 2006, doi: 10.1016/j.anucene.2005.12.005.

[4] *Post-irradiation Examination and In-pile Measurement Techniques for Water Reactor Fuels*, IAEA-TECDOC-CD-1635, IAEA, Vienna, Austria, 2009.

[5] D. Reilly, N. Ensslin, H. Smith, Jr., and S. Kreiner, "Passive nondestructive assay of nuclear materials," Los Alamos Nat. Lab. Rep., Los Alamos, NM, USA, Tech. Rep. LA-UR-90-732, 1991.

[6] I. Matsson, B. Grapengiesser, and B. Andersson, "LOKET—A gamma-ray spectroscopy system for in-pool measurements of thermal power distribution in irradiated nuclear fuel," *Nucl. Instrum. Methods Phys. Res. A, Accel. Spectrom. Detect. Assoc. Equip.*, vol. 569, no. 3, pp. 872–882, Dec. 2006, doi: 10.1016/j.nima.2006.08.103.

[7] C. T. Nguyen *et al.*, "Monitoring burn-up of spent fuel assemblies by gamma spectrometry," *IEEE Trans. Nucl. Sci.*, vol. 60, no. 2, pp. 1107–1110, Apr. 2013, doi: 10.1109/TNS.2013.2241790.

[8] S. Holcombe, P. Andersson, S. J. Svärd, and L. Hallstadius, "Determination of the rod-wise fission gas release fraction in a complete fuel assembly using non-destructive gamma emission tomography," *Nucl. Instrum. Methods Phys. Res. A, Accel. Spectrom. Detect. Assoc. Equip.*, vol. 837, pp. 99–108, Nov. 2016, doi: 10.1016/j.nima.2016.08.061.

[9] P. Andersson, S. Holcombe, and T. Tverberg, "Inspection of a LOCA test rod at the Halden reactor project using gamma emission tomography," in *Proc. Top Fuel Light Water React. Fuel Perform. Meeting*, Boise, ID, USA, Sep. 2016, pp. 1–12. [Online]. Available: http://urn.kb.se/resolve?urn=urn:nbn:se:uu:diva-303810

[10] A. Hedin, "Spent nuclear fuel—How dangerous is it? A report from the project 'description of risk'," Swedish Nucl. Fuel Waste Manage., Stockholm, Sweden, Tech. Rep. SKB-TR–97-13, 1997. [Online]. Available: http://inis.iaea.org/Search/search.aspx?orig_q=RN:29015601

[11] L. A. Currie, "Limits for qualitative detection and quantitative determination. Application to radiochemistry," *Anal. Chem.*, vol. 40, no. 3, pp. 586–593, Mar. 1968.

[12] J. Leppänen, M. Pusa, T. Viitanen, V. Valtavirta, and T. Kaltiaisenaho, "The serpent Monte Carlo code: Status, development and applications in 2013," *Ann. Nucl. Energy*, vol. 82, pp. 142–150, Aug. 2015.

[13] C. J. Werner, "MCNP users manual—Code version 6.2," Los Alamos Nat. Lab., Los Alamos, NM, USA, Tech. Rep. LA-UR-17-29981, 2017.

[14] L. Senis *et al.*, "Evaluation of gamma-ray transmission through rectangular collimator slits for application in nuclear fuel spectrometry," *Nucl. Instrum. Methods Phys. Res. A, Accel. Spectrom. Detect. Assoc. Equip.*, vol. 1014, Oct. 2021, Art. no. 165698, doi: 10.1016/j.nima.2021.165698.

[15] V. Rathore, L. Senis, E. A. Sundén, P. Jansson, A. Håkansson, and P. Andersson, "Geometrical optimisation of a segmented HPGe detector for spectroscopic gamma emission tomography—A simulation study," *Nucl. Instrum. Methods Phys. Res. A, Accel. Spectrom. Detect. Assoc. Equip.*, vol. 998, May 2021, Art. no. 165164.

[16] V. Rathore *et al.*, "Calculations of the spatial response of a collimated segmented HPGe detector for gamma emission tomography by MCNP simulations," in *Proc. ANIMMA*, Prague, Czech Republic, 2021, doi: 10.1109/TNS.2022.3152056.

[17] C. J. Werner, "MCNP(R) user's manual coder version 6.2," Los Alamos Nat. Lab., Los Alamos, NM, USA, Tech. Rep. LA-UR-17-29981, 2017.

[18] G. R. Gilmore, *Practical Gamma-Ray Spectroscopy* (Nuclear Training Services). Warrington, U.K.: Wiley, 2008.

[19] H. Takiishi, J. H. Duvaizen, I. M. Sato, J. L. Rossi, L. A. T. Pereira, and L. G. Martinez, "Recycling of Zircaloy machining chips by VAR remelting and powder metallurgy techniques," *Mater. Sci. Forum*, vols. 727–728, pp. 356–361, Aug. 2012, doi: 10.4028/www.scientific.net/msf.727-728.356.

[20] H. Sonnenburg *et al.*, "Report on fule fragmentation, relocation, dispersal," OECD, Paris, France, Tech. Rep. NEA/CSNI/R(2016)16, 2016. [Online]. Available: https://www.oecd-nea.org/jcms/pl_19748/report-on-fuel-fragmentation-relocation-dispersal-ffrd?details=true

[21] G. F. Knoll, *Radiation Detection and Measurement*. New York, NY, USA: Wiley, 1979.